



Review of mechanical properties of and optimisation methods for continuous fibre-reinforced thermoplastic parts manufactured by fused deposition modelling

Michael Handwerker^{1,2} · Jörg Wellnitz² · Hormoz Marzbani¹

Received: 4 June 2020 / Accepted: 19 April 2021 / Published online: 9 May 2021
© The Author(s) 2021

Abstract

A new way of manufacturing continuous fibre-reinforced plastics is the embedding of fibres in the filament of a 3D printer. This method could be used in manufacturing composite materials with a thermoplastic matrix containing glass, Kevlar and carbon fibres. This paper provides an overview of research on the mechanical and physical properties of these parts as well as optimisation approaches of additively manufactured thermoplastics. Furthermore, applicable testing and analysis methods and their corresponding standards are included. Several studies, which represent the current state of the art, are reviewed in detail for the analysis of the mechanical performance of different fibre reinforcements. In addition, an overview of different optimisation approaches is given. The ultimate tensile strength of Kevlar and glass fibre-reinforced parts are similar to those of common Aluminium alloys whereas the carbon fibre reinforced parts outperform their aluminium counterparts. Major performance limitations include a poor adhesion between layers as well as a high air void ratio.

Keywords Fused filament fabrication · Fused deposition modelling · Continuous fibre · Thermoplastics

1 Introduction

In recent years, design and manufacturing of lightweight structures have gained more importance. Especially in the aviation and automotive industry, the requirement for lower emissions and greater range has led to the development of new technologies for the manufacturing of lightweight materials. Looking back in history, steel was replaced by aluminium which is now getting competition from composite materials [1]. The most noted representative of such composite materials are fibre-reinforced plastics. The performance of these non-isotropic materials mostly depends on fibre orientation, fibre content, the type of plastic/fibre used and the manufacturing process [2]. Most used composite materials in the aviation industry are carbon fibres with a thermosetting polymer matrix. These high-performance composites

are manufactured by stacking epoxy infused layers of uni-directional fibre mats (prepregs) on top of a mould and then curing it by applying pressure and high temperatures [1].

A new method for producing fibre-reinforced plastics is the use of fused deposition modelling (FDM) sometimes also referred to as fused filament fabrication (FFF). In this process, a thermoplastic filament is molten, extruded through a nozzle and deposited on the growing work. The required composite materials are created by adding continuous fibres to the filament. This manufacturing process gives engineers a lot of design flexibility and allows to produce optimised high-performance parts with complex geometries without requiring moulds or autoclaves. As a result, this process is a step towards the “print-it-all” fabrication process, since poor mechanical performance has been limiting the areas of application for 3D-printed plastic materials [3]. Of course, issues such as the high production time, the high costs and slow certification processes still need to be addressed before additive manufacturing can be used in large-volume productions [4].

In the present study, the material properties of these additively manufactured composites as well as optimisation techniques that allow for tailored fibre placement will be reviewed.

✉ Michael Handwerker
Michael.Handwerker@thi.de

¹ Royal Melbourne Institute of Technology, Plenty Road,
Bundoora, VIC 3083, Australia

² Technische Hochschule Ingolstadt, Esplanade 10,
85049 Ingolstadt, Germany

2 Commercial printers

There are two basic working principals in processing continuous fibres using the FDM process. The continuous fibre used for reinforcement is either already present in the filament or fed into the nozzle separately. A summary of currently available FDM printers with the ability to process continuous fibre reinforcements is shown in Table 1. Markforged was the first company to sell an FDM printer capable of processing continuous fibre reinforcements in 2014 with a second generation released in 2016. The main restrictions of these two printers are the closed source software which dictates the fibre path and the fact that only the manufacturer's filament can be processed [5]. The Anisoprint Composer A3 and A4, which were released in early 2020 are almost the opposite. They mix the filament and fibres in the printing head and allow any materials to be used. Their software also allows adjustment of the fibre path and nozzle temperature [6]. This makes the Anisoprint composer perfect for research purposes since the influence of many factors could be investigated. Judging by the available information, the major difference between the Desktop Metal printer and the Markforged printer is the matrix material. Markforged uses polyamide and an unspecified amorphous plastic, whereas the Desktop Metal printers can process polyether ether ketone (PEEK) and polyetherketoneketone (PEKK) which both are plastics that can be used at higher temperatures than conventional plastics [7]. For manufacturing bigger structures, the CEAD CFAM Prime is currently the only option [8]. Since the Markforged printers were released to the market almost 6 years ago, most of the cited studies in this work used these printers.

3 Mechanical performance

It is important to state the testing direction when discussing the mechanical performance of composite materials. The system shown in Fig. 1 is used for the present study. “X1” refers to the fibre direction, “X2” is perpendicular to the

fibres and parallel to the printing bed and “X3” is perpendicular to both the fibres and the printing bed.

An important property for composite materials is the shear strength. It can be distinguished between intra- and interlaminar shear strength with continuous fibre reinforced plastics. The former refers to shear stresses within one layer and thus effects the fibres, matrix as well as the fibre matrix bond. The latter refers to shear stresses between layers, which leads to delamination [9,10].

When conducting fatigue tests, it is important to take the testing frequency into consideration. Tests on long fibre-reinforced plastics have shown that the fatigue strength decreases when increasing the testing frequency. This behaviour was attributed to hysteretic heat as well as the low thermal conductivity of thermoplastics [11]. Furthermore, it was found that creeping relaxes local stress accumulations, and therefore, has an influence on the durability [12]. Experiments conducted with thermosetting short glass fibre-reinforced composites have shown that many factors, like the manufacturing parameters, testing conditions and materials have an influence on the predicted lifetime, so it is important to state these conditions, when publishing test results [13]. Table 2 contains a summary of mechanical test methods, the information that can be obtained as well as corresponding standards.

As mentioned in the previous section, Markforged was one of the first companies to release a 3D printer that can process continuous fibre filament. This is the reason why their printers are used in most of the published research projects to date. Unless otherwise stated, the mechanical properties refer to parts manufactured by Markforged printers.

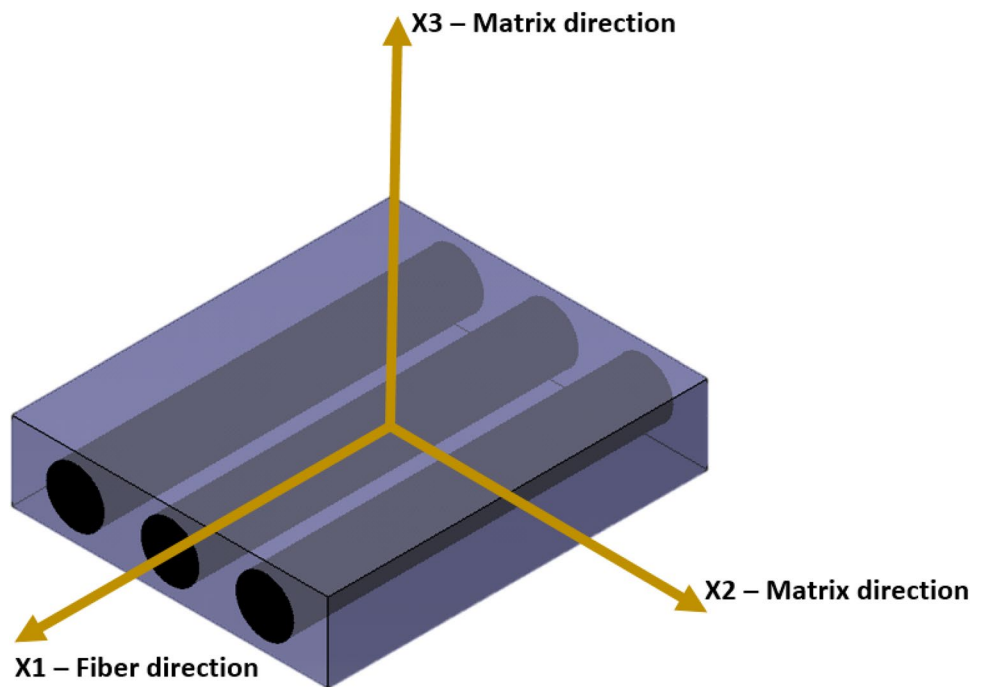
3.1 Kevlar fibre

3.1.1 Tensile and flexural testing

The tensile strength and Young's modulus of Kevlar-reinforced parts were determined by Melenka et al. according to ASTM D638-14 [39]. The work compared samples with varying number of reinforced rings. A maximum ultimate tensile strength (UTS) of 80 MPa was determined with

Table 1 Commercial FDM printers that can process continuous fibre reinforcement

Company	Markforged [5]	Anisoprint [6]	CEAD [8]	Desktop metal [7]
Printer	Mark One/Two	Composer A4/A3	CFAM Prime	Fibre series
Software type	Closed source	Open source	Closed source	Closed source
Build volume (mm ³)	320 × 132 × 154	297 × 210 × 140 420 × 297 × 210	2000 × 4000 × 1500	310 × 240 × 270
Fibre material	Carbon, Glass and Aramid	Open material system	Carbon and Glass	Carbon and Glass
Working principle	Impregnated filament	Mixer Head	Mixer Head	Impregnated filament
Available since	2014/2016	Early 2020	2018	Early 2020

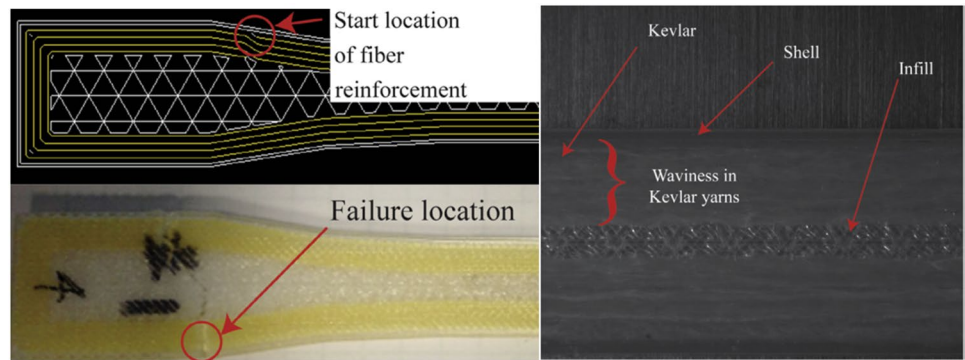
Fig. 1 Coordinate system for fibre-reinforced parts**Table 2** Summary of test methods, their resulting information as well as applicable test standards

Method	Resulting information	Standards
Tension, compression	Stress–strain behaviour, yield strength, ultimate strength, Young’s modulus	ASTM D3039 [14] ASTM D6641 [15] ASTM D3410 [16] ASTM D6484 [17] ASTM D5766 [18] ASTM D6742 [19] ASTM 6264 [20] ISO 527-4 [21] ISO 12817 [22] ISO 14126 [23] ISO 11566 [24]
Shear	Shear-stress–strain behaviour, shear modulus, shear strength	ASTM D5379 [25] ASTM D2344 [26] ASTM D3518 [27] ASTM 5467 [28] ASTM D4255 [29] ASTM D3846 [30] ISO 14130 [31] ISO 14129 [32] ISO 15310 [33]
Flexural	Flexural stress–strain behaviour, flexural modulus, flexural strength	ASTM D7264 [34] ASTM D6272 [35] ASTM D6415 [36] ISO 14125 [37]
Fatigue	Fatigue behaviour	ASTM D3479 [38]

two layers being reinforced by five rings each. Because the start of the fibre path was in a high stress area, the determined values do not represent the full potential of the material and the authors recommend not to place

the starting point of the fibre in the load path. Through optical microscopy, a waviness in the Kevlar yarns was observed which is suspected to be caused by a lack of tension on the fibres during the printing process. These

Fig. 2 Location of the point of failure (left) and waviness of the Kevlar fibres (right) [39]



effects are both shown in Fig. 2. Once the load is applied, the fibres straighten which explains the observed non-linear stress–strain behaviour. Besides the acknowledged flaw of the starting point of the fibre being in the load path, the applied standard is not intended for reinforced plastics.

A similar test setup was used by Dickson et al. applying the ASTM D3039 standard for tensile tests [40]. With 8 out of 32 layers reinforced a UTS of 164 MPa and a Young's modulus of 6.7 GPa was measured. To avoid the start and end point of the fibre within the load path, the fibre ends were laid beyond the tabbing points. After the test, barely any residue of the matrix material could be found when examining the Kevlar fibres, which is an indicator of a weak bond between the matrix material and the fibre. The flexural strength and modulus with eight out of 32 layers being reinforced was 125.8 MPa and 6.65 GPa.

Adabi et al. [41] found the main failure in tensile tests to be fibre tensile damage which showed as an almost lateral failure of the test piece. With 12 out of 25 layers being reinforced in load direction an average UTS of 150 MPa and a Young's modulus of 8.7 GPa was determined.

3.1.2 Impact behaviour

V-notch test pieces and plates were used for Charpy testing and shot with a gas gun by Scrocco et al. [42] to determine the impact behaviour of continuous Kevlar-reinforced FDM parts. Two reinforced layers perpendicular to the notch in a test piece designed according to ASTM E23 [43] resulted in an impact energy of 11.38 J. When the reinforced layers were parallel to the notch no significant strength increase was found. In addition, 6-mm-thick plates were shot with spherical bearings at velocities between 208 and 255 m/s with varying reinforcement. The projectiles managed to penetrate 2 mm of the Kevlar reinforcement at 208 m/s and the plate was very close to stopping the projectile travelling at 255 m/s.

3.2 Glass fibre

3.2.1 Tensile and flexural testing

Dickson et al. [40] determined the UTS of continuous glass fibre-reinforced test specimens depending on the fibre content. It was observed that more fibre reinforcement does not lead to a proportional increase in UTS. This was suspected to be caused by air inclusions that got bigger and more frequently occurred as more fibres were used. 30 out of 32 layers reinforced resulted in an ultimate tensile strength of 444 MPa which exceeds the strength of Aluminium 6061-T6.

An average UTS of 450 MPa and Young's modulus of 7 GPa was determined by Goh et al. [44] according to ASTM D3039. During tensile testing, the specimens showed a sudden drop in tensile stress followed by slight rise before the sudden failure of the test piece, which is suspected to be caused by local fibre failure. Tensile and shear rupture were the failure modes causing fibre breakage. Fibre pull-out also was observed but was found to be insignificant compared to the fibre breakage. Delamination and de-bonding at the layer interfaces were observed, which indicates a weak bonding between adjacent layers. The fibre volume fraction of 35% was determined by burning of the matrix.

Justo et al. [45] determined an average UTS of 701 MPa and a Young's modulus of 68 GPa according to ASTM D3039 by extracting test pieces from a plate with the failure occurring simultaneously in both the centre and close to the tabs. The number of reinforced layers is not stated and microscopic analysis revealed almost no waviness in the fibre paths but air gaps within the composite were observed.

An average flexural strength of 149 MPa and flexural modulus of 15 GPa was determined by Goh et al. [44] according to ASTM D790. Testing showed that the flexural strength gradually decreased after reaching a 1% strain. This is because individual localised buckling occurred in the compression layers due to the poor bonding of the layers which resulted in sequential failure of individual layers. Goh et al. suspects printing parameters used to manufacture the

samples to be the cause of this behaviour and similar results were obtained by Dickson et al. [40].

3.2.2 Shear testing

Samples with a $\pm 45^\circ$ pattern were used by Justo et al. who determined the shear strength according to ASTM D3518 to be 67 MPa and the shear modulus to be 0.88 GPa [45]. The stress–strain graph revealed two phases. A convex phase that is caused by the fibres aligning themselves in load direction (scissor effect) followed by a concave phase that lasts until failure. The authors contributed that effect to the high strain as well as fibre pull-out. It was also observed that the failure zone decreased in width by 23%.

3.3 Carbon fibre

3.3.1 Tensile and flexural testing

The UTS determined by Dickson et al. [46] for samples with 8 out of 26 layers being reinforced in a concentric pattern was 216 MPa with a Young's modulus of 13 GPa. Fibre pull-out was found to be the main cause of the failure and optical microscopy showed remaining residue on the carbon fibres suggesting a strong bond to the matrix. Air inclusions that have a negative effect on the parts performance are shown in Fig. 3. Their number and size increased with the fibre fraction.

Blok et al. [47] tested unidirectional samples which were cut out of a concentric printed plate with a fibre volume fraction of 27%. The average UTS was determined to be 986 MPa and the average Young's modulus to be 63 GPa. Since these values are higher than the ones stated by the manufacturer and other researchers, a measurement error is

very likely. High-frequency fibre noise was audible at low stresses which did not occur again before failure. Waviness of the fibre strands is suspected to be the cause of the slight increase in stiffness with the load. The air voids reported by Dickson et al. between tracks and within them were also observed.

Van der Klift et al. [48] tested samples that were cut out of a plate which resulted in an average UTS of 464 MPa and a Young's modulus 36 GPa with six out of ten layers reinforced. The UTS varied between 138 and 171 MPa with two out of ten layers reinforced. It was also found that the number of voids increased when the fibre volume was increased.

When only partially reinforcing a part, the continuous fibres can either be stacked or placed all within a couple of layers. Lozada et al. [49] found that placing the fibres within one layer rather than stacking them results in higher UTS. A definite explanation could not be found, but the stacked specimens showed non-uniform wetting of the fibres. A fibre volume fraction of 54% led to a UTS of 310 MPa and a Young's modulus of 24 GPa, which were determined according to ASTM D638.

An average UTS of 600 MPa and Young's modulus of 13 GPa was determined by Goh et al. [44] with a fibre volume fraction of 41%. The amount of fibre pull-out was found to be insignificant compared to the fibre breakage which means, a good fibre matrix bond exists. A CT scan of the specimen revealed that there are air voids between adjacent layers (Fig. 4) as well as air voids within the filament.

For specimens reinforced with six out of ten layers the average UTS was determined to be 493.9 MPa and the Young's modulus to be 45 GPa in accordance with ASTM D3039 [50]. With the fibres aligned 90° to the load direction the average UTS was 14 MPa with a Young's modulus of 3.5 GPa. The ratio of longitudinal elastic modulus to fibre

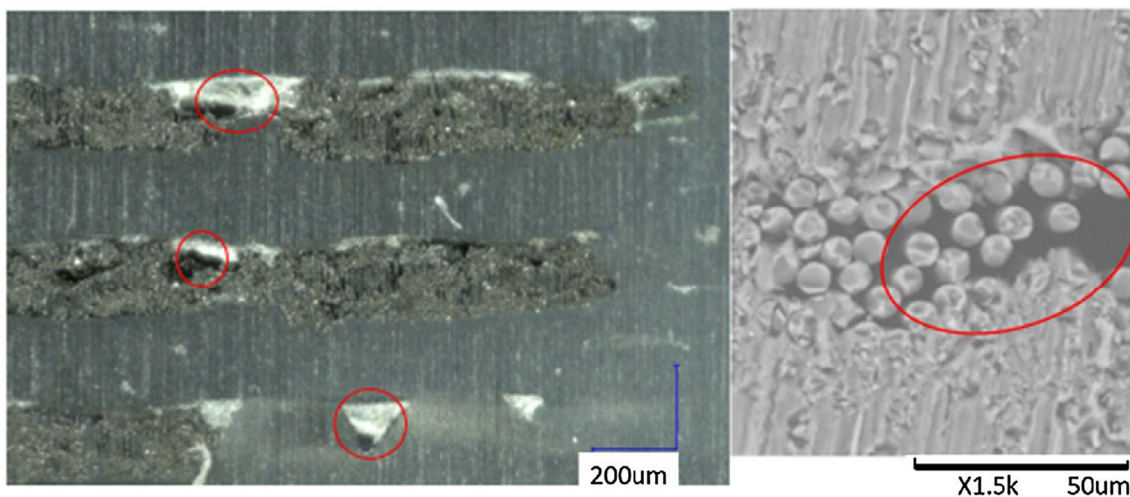


Fig. 3 Air inclusions seen through an optical (left) and electron (right) microscope [46]

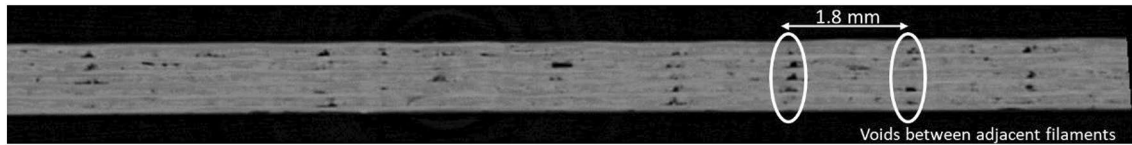


Fig. 4 Air voids between adjacent filaments [44]

volume is found to be the same as for conventional thermo-setting composites.

Adabi et al. [41] found the main failure in tensile tests were both tensile and shear stresses. This was supported by test pieces breaking under an angle. An average UTS of 330 MPa and a Young's modulus of 37 GPa was determined with ten out of 20 layers being reinforced.

Using the JIS K7075-1991 standard Todoroki et al. [51] determined the fibre volume fraction to be 30%. Samples tested with a displacement speed of 0.5 mm/min showed a tensile strength of 701 MPa and a Young's modulus of 61 GPa. When comparing the UTS' perpendicular to the fibre direction it was found that the bond between strands within one layer is stronger than the bond between layers. It is suspected that the heat flow from the printing nozzle did not reach the underlying layer but rather got distributed along the filament because of the high thermal conductivity of the fibres. This resulted in a 75% drop in strength and a 40% drop in stiffness when comparing the "X2" and "X3" testing direction and the air void ration increased from 7 to 11.3%. It is mentioned that a future study will investigate this phenomenon by simulating the printing process. A slightly offset or uneven printing bed that reduces the nozzle pressure was stated as an additional possible cause.

Blok et al. [47] tested specimens with 0° fibre orientation according to ASTM D7264. An average flexural strength of 485 MPa and a flexural modulus of 42 GPa were determined with 30 out of 32 layers being reinforced. Limiting factors for the mechanical performance were found to be a poor fibre matrix bond as well as a high void content acting as premature failure initiators.

Similar results were obtained by Goh et al. found the average flexural strength to be 430 MPa and the flexural modulus to be 38 GPa [44]. At 1% strain the flexural stress experienced a little drop before rupturing. The initiation of the crack that caused the failure was caused by the high compressive stress at the upper most surface which crushed the fibres and it propagated towards the neutral axis. When it reached the tensile side of the fibres, the stress became too high and the specimen ruptured. This behaviour is not unique to additively manufactured composites but is the same for conventional fibre-reinforced plastics.

Zhang et al. [52] used a custom build FDM printer with an integrated roller, that applied pressure and heat right after the filament was extruded. It was found that this procedure

will increase the mechanical performance, but too much pressure will cause a poor surface quality or even lead to printing failure. Carbon fibre-reinforced samples with a PLA matrix achieved a maximum UTS of 645 MPa. Judging by the pictures provided in the article, this procedure is not yet on the level of commercial printers but still proves it could address the shortcomings of the FDM process.

3.3.2 Shear testing

Todoroki et al. [27] used $\pm 45^\circ$ samples to calculate the shear strength according to JIS K7019, which is the Japanese equivalent of the ASTM D3518 standard. A comparison between test pieces with their edges cut off and samples with a serpentine pattern revealed better results with the former. A shear strength of 90/52 MPa and shear moduli of 2.2/2.1 GPa were calculated. Since a rotation of fibre bundles to a lower angle was observed, the actual shear strength is lower [51].

3.4 Interlaminar shear testing

Caminero et al. examined the Interlaminar shear behaviour of parts reinforced with continuous Kevlar®, glass and carbon fibres according to ISO 14130 [53]. The two different types of reinforced samples used are shown in Fig. 5. Table 3 contains the number of reinforced layers for each of the different reinforcement materials and type of test pieces.

The results of the test are shown in Fig. 6. As can be seen in Fig. 6a, the interlaminar shear strength increases for both glass and carbon fibre when increasing the fibre volume fraction, but the increase was not proportional to the added fibres. According to Caminero et al. [53] this is most likely due to the increase in air gaps which have also been reported in other works. The reason for the shear behaviour of the Kevlar-reinforced samples is poor wettability of the Kevlar fibres which leads to a poor bonding between the matrix and the fibre. The thermosetting prepreg with a fibre volume of 59% vastly outperforms the additive manufactured parts mainly because of the thermosetting matrix material as well as manufacturing process itself. The prepreg is processed in an autoclave under high pressure, which minimises air gaps, whereas the additive manufactured materials are processed under atmospheric pressure. In addition, the prepreg cures

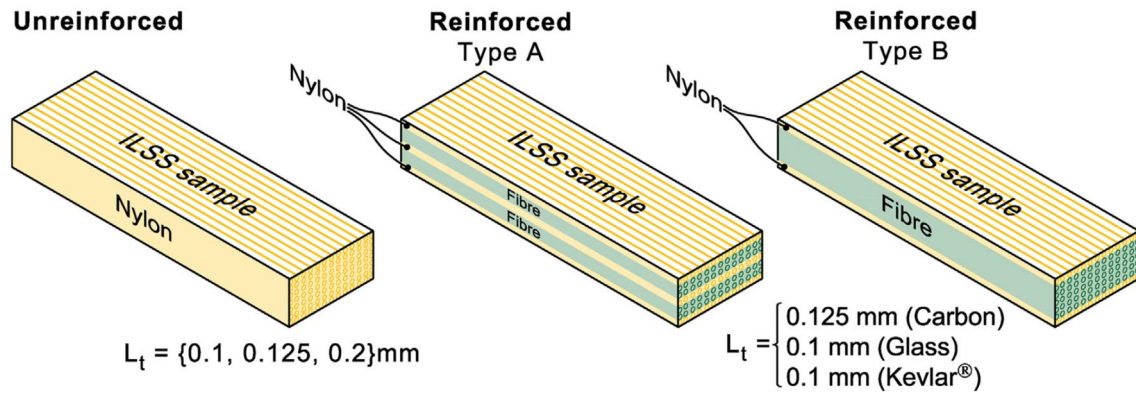


Fig. 5 Test pieces used by Caminero et al. [53]

Table 3 Amount of reinforced fibre layers out of the total layers of fibre for each type of test piece [53]

	Type A	Type B
Carbon fibre	18/48	46/48
Kevlar® fibre	22/60	58/60
Glass fibre	22/60	58/60

as one piece whereas the FDM-produced parts are built layer by layer.

3.5 Fatigue testing

With a load ratio of 0.1, Imeri et al. [54] evaluated the number of load cycles until failure according to ASTM E606M. The specimens were either reinforced with up to three concentric rings, an isotropic reinforcement with fibres oriented in load direction or a combination of both. The load was varied in four steps and the number of cycles until failure

was measured. Due to the testing equipment they used only cycles up to 10,000 could be detected. Even though the acquired data did not suffice for a reliable fatigue prediction model it was shown that the fill pattern has an influence on the fatigue performance. The isotropic fill pattern resulted in the highest number of endured load cycles. As in the UTS experiments, carbon fibre was the strongest and Kevlar the weakest. An increase in fibre content lead to an increase of the fatigue performance. While this work shows some correlation factors, its main flaw is the use of the ASTM E606 standard. Due to the “dog bone” shape of the test pieces, the concentric reinforced samples were destined to perform worse than the isotropic reinforced ones. The fibre direction is not oriented in the load direction in the tapered part of the test piece. This would have not been an issue if rectangular test pieces (ASTM D3479) had been used.

Pertuz et al. also investigated the influence of different printing patterns and fibre orientations (0° , 45° , 60°) on

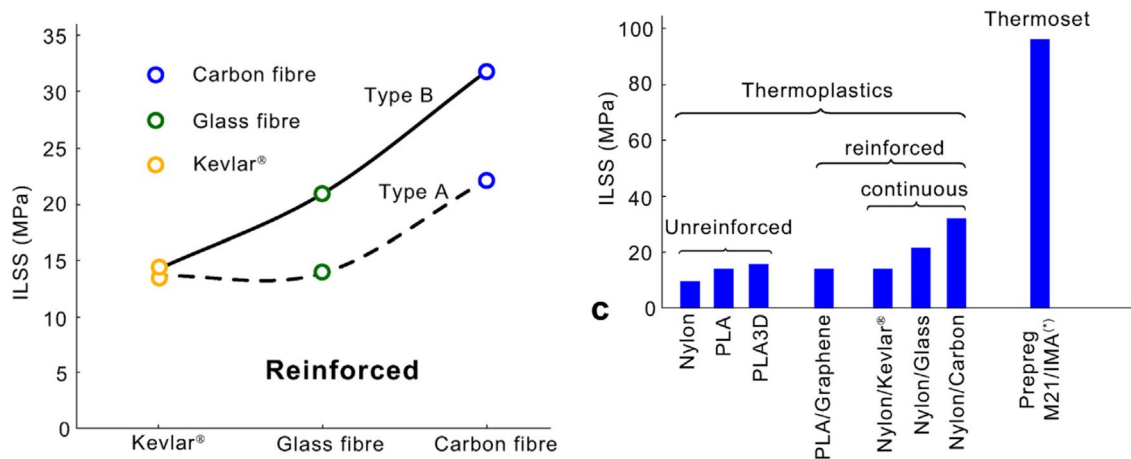


Fig. 6 Average maximum interlaminar shear strength (ILSS). a The influence of fibre volume on ILSS. b Comparison of additive manufactured materials and pre-impregnated M21/MMA (thermosetting) [53]

the fatigue behaviour according to ASTM D7791 [55] with a load ratio of 0.1 [56]. Samples with fibres orientated in load direction were loaded with 95%, 90%, 85% and 80% of their ultimate tensile strength and the number of cycles until failure were measured. While the Kevlar and glass fibre-reinforced samples only lasted a maximum of 550 and 2500 cycles, respectively, the carbon fibre reinforced samples lasted up to 97.000 cycles at 80% of the ultimate tensile strength. Furthermore, the influence of the fibre angles was tested using glass fibre specimens. Samples were loaded under the same conditions as before. It was observed that with greater angles the matrix material absorbs most of the load, which lead to a very low fatigue resistance. The obtained data were fitted to Basquín's fatigue model for each of the tests. Unfortunately, the applied standard also uses "dog bone" shaped samples that have variations in the cross-sectional area. The authors themselves stated that "a considerable number of specimens [...] broke in the change of the transversal area section". As with Imeri et al., this indicates that the mentioned location is a weak spot and the obtained data is only useful for samples that did not have curved fibre paths.

4 Material analysis

One of the most common procedures to analyse the thermal behaviour of a plastic is the differential scanning calorimetry (DSC). DSC measures the heat energy required to increase the temperature of a material, which allows the determination of the melting and glass-transition temperatures, the degree of crystallinity, cold crystallisation processes, impurities as well as the effect of additives [57].

Another way to determine the glass-transition temperature as well as the viscoelastic behaviour of polymers is the dynamic mechanical analysis (DMA). A small load is applied in a cyclic manner and changes in stiffness and damping are measured. When the temperature is increased, the material stiffness will decrease and the viscosity significantly increases, when the glass-transition temperature is reached [58].

For evaluation of the thermal stability and the fibre content, thermogravimetric analysis (TGA) can be applied. The TGA procedure measures the sample mass by a micro-scale as a function of time or temperature. Dynamic thermogravimetry refers to a linear increase of the temperature, which will lead to different constituents of the material deterioration at different times/temperatures. As a result, the mass loss at a certain temperature allows reaching conclusions about the material composition [59]. Static thermogravimetry, where the temperature is held at a certain level, can also be used to burn off the matrix material. If this process is taking place under an inert atmosphere,

it is referred to as pyrolysis [60]. Another way of determining the fibre volume fraction is by matrix digestion. In this procedure, the matrix material is dissolved by a heated-up acid. The fibres are then dried and weighed. Since the weight of the total composite and the densities of the materials are known, the fibre volume fraction can be calculated with those values [61].

A very important aspect for composites manufactured by FDM is the determination of the air void content, which can be determined by comparing the theoretical density of a material with the actual density. The actual densities are obtained by burning off the matrix like it is done with the pyrolysis process [62]. However, this method does not give any information about the void sizes and their distribution. X-ray microtomography can be used to obtain this important information. It can furthermore be used to visualise cracks and fibre distribution. A detailed description of how polymer composites can be analysed using this technique can be found in [63].

A summary of these test methods and their corresponding international standards are listed in Table 4.

An in-depth filament review of the raw filament for the Markforged printer was conducted by Pascual-Gonzalez et al. [77]. DSC analysis showed that the glass and aramid fibres are embedded in polyamide 6, whereas the carbon fibres are embedded in an unspecified amorphous plastic. With 4.8%, the aramid filament had the highest water content and with 2.1% the carbon filament had the least, followed by glass fibre with 2.6%. Digestion, pyrolysis and TGA were used to determine the fibre content. The sulphuric acid, that was used for digestion also dissolved the aramid fibres, which rendered this method useless for this type of fibre. Pyrolysis led to a high scattering of the determined values. Fibre volume fractions determined by TGA were 31.7% for the glass fibre, 40.4% for the aramid fibre and 36.4% for the carbon fibre filament. These values are a little bit higher than values determined by the authors of [44, 50, 51]. The discrepancy may be a result of the fibre density, which was not known and had to be estimated by all the authors. While they found air voids in the raw filament, they concluded that the high crystallisation temperature of polyamide, which was determined to be 160 °C, may also have an influence on the weak layer adhesion and the poor mechanical performance [77].

Qinghao et al. [78] analysed the influence of the air voids on the mechanical performance. By heating up the printed test pieces in a mould above their melting point (230 °C) and applying pressure (5 MPa). The air void ratio went down from 12 to 6% as a result. This resulted in a 93% increase of the flexural strengths. Even though the strength increase was significant, this investigation has a purely scientific benefit. Because the use of a mould press would eliminate the great benefit of additive manufacturing. In addition, it was not

Table 4 Summary of calorimetric and chemical procedures to analyses composite materials, the information that can be obtained using those methods and the corresponding standards

Method	Resulting information	Standards
DSC	Glass-transition temperature, melting temperature, degree of crystallinity, plastic identification	ASTM D3418 [64] ASTM E1356 [65] ISO 11357 [66–70]
DMA	Glass-transition temperature, viscoelastic behaviour	ASTM D7028 [71]
TGA	Thermal stability, material composition, fibre volume fraction	ASTM E1641 [72] ASTM E1131 [73] ISO 11358 [74]
Matrix digestion, pyrolysis	Fibre volume fraction, air void ratio	ASTM D3171 [61] ASTM D2734 [62] ISO 11667 [75]
Microtomography	Air void ratio and crack, size and distribution; fibre alignment	ASTM E2533 [76]

clear, if the strength increase could be attributed to the high temperature or the applied pressure.

5 Optimisation and failure criteria

In automated processes, as mentioned in the introduction, conventional fibre-reinforced plastics are usually manufactured by stacking unidirectional fibre mats on top of a mould and then cured under pressure and temperature. This means that the fibre orientation cannot be chosen at will by the engineer, since all fibres within one layer are aligned in the same direction.

If composite parts are manufactured by FDM, the individual fibre paths can be defined during the development process. It is a well-known fact that composite materials containing continuous fibres are the strongest, when loaded in fibre direction (on-axis loading). If the load is applied at an angle (off-axis loading), the strength decreases since the significantly weaker matrix material experiences higher stresses [79]. For a maximum utilisation of the fibres, they must be positioned in a way that leads to a high tensile stress for the fibres (on-axis load). In a complex multilayered part, this is impossible to do by hand, so computer-based optimisation processes are required.

It can be differed between approaches that model the fibre through parameterised curves (curve-based designs) and approaches where the finite elements contain information about material orientation (element-wise designs). The difference between the two is shown in Fig. 7. Since this topic is worth an independent review paper, only a brief overview of recent work will be given.

With element-wise design, each element is assigned a parameter, that represents the fibre orientation. As a result, the stiffness of the element regarding a certain direction can be changed by changing the fibre orientation [80, 81]. As shown in Fig. 7, at the beginning of the process,

the fibres in each element (represented by the lines) are aligned at random. The optimisation process determines the ideal fibre orientation for each element. Post processing is required to transfer the individual element orientations into homogenous fibre paths [82]. To reduce the calculation time, the fibre orientation can be limited to a pre-defined number of values [83, 84]. The discrete material optimisation (DMO) method developed by Lund [83] uses a matrix containing a pre-defined number of fibre orientations to limit the number of possible orientations. While the DMO theoretically allows an unlimited number of orientations, the shape function with penalisation (SFP) approach is limited to four fibre orientations: 0° , $\pm 45^\circ$ and 90° [85]. SFP uses the shape functions of the finite elements as weights to determine the optimal fibre orientation. The SFP was later extended to allow the use of eight fibre orientations [86]. A similar approach was taken by Gao et al. [87]. A different approach is to align the fibres along the principal stress directions. Malakhov et al. and Zhu et al. applied this principal to determine the fibre paths in structures with geometric discontinuities, such as holes and notches [88, 89].

Curve-based optimisation processes on the other hand use parameterised curves that represent the fibre paths [90]. Contrary to element-wise optimisation, no post-processing is required since the curves already represent the fibre paths. Figure 7 illustrates this with the example of an additively manufactured lug that is loaded with compression inside the hole. Cubic splines with five parameters are used. The failure mode was evaluated using Hashin's failure criteria (comp. next paragraph) [91]. An approach inspired by fluids dynamics was perused by Yamanaka et al. [92]. They used streamlines that are usually used to model the flow of a fluid as a representation of the fibre path. The Tsai–Wu criterion was used to evaluate the material failure. This procedure was used to optimise a composite plate with a hole in the middle. Compared to a uniaxially reinforced ply, the optimised part

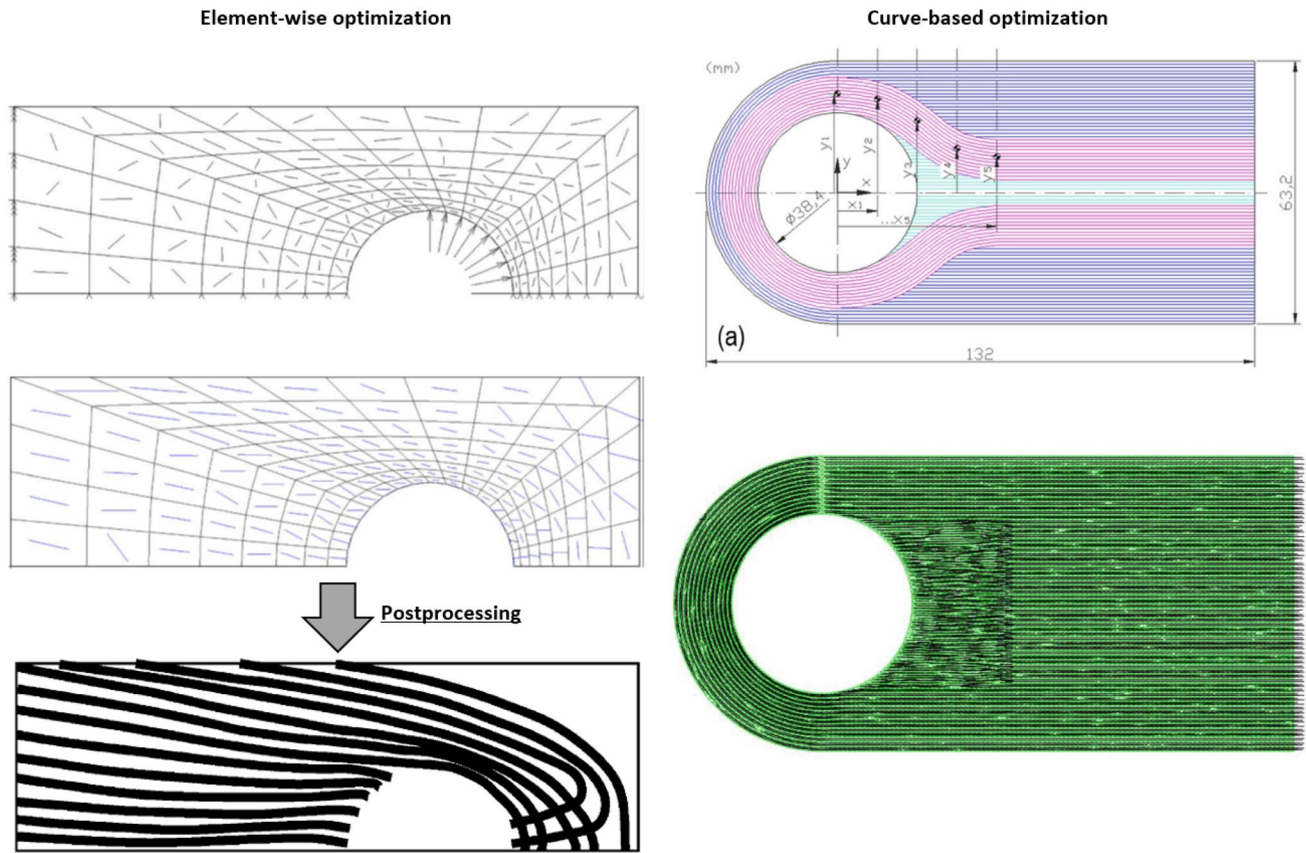


Fig. 7 Difference between element-wise optimisation [82] (left) and fibre path optimisation [91] (right)

showed a strength increase of 28%. A summary of these different optimisation approaches can be found in Table 5.

To optimise any part, the point of failure must be known. Contrary to isotropic materials like metals composite laminates cannot be designed using equivalent tensile stresses (e.g. von Mises stress) to calculate the failure under combined loads. This is because the matrix and fibres have vastly different physical properties resulting in different stresses under load. A composite material can either experience fibre failure or inter-fibre failure. When many fibres in a layer break, it is referred to as fibre failure. It is caused by high tensile or compression stresses. This failure mode is unacceptable because it leads to high stresses in adjacent layer which causes delamination and there for a complete part failure. Inter-fibre failure on the other hand can be a tolerable damage, depending on the kind of the stress that caused it. A compressive stress perpendicular to the fibres causes, for a brittle matrix material, a shearing off the layer. That layer starts acting like a wedge when further increasing the compressive stress making the whole part burst. Other stresses, like shear or tensile, will cause different kinds of matrix cracks. These cracks usually penetrate the whole layer and are only stopped when reaching a layer with a different fibre

orientation. All inter-fibre failures have in common, that the fibre does not get damaged. Up to a certain amount, inter-fibre failure is tolerable [95].

To determine, whether a certain combination of loads leads to either fibre failure, inter-fibre failure or is tolerable, advanced failure criteria are required. In previous works that analysed the failure of continuous fibre reinforced parts manufactured by fused filament fabrication the Hashin's and Tsai-Wu criterion were used to take this effect into account [41, 91]. Hashin's criterion is simple to use, because it only relies on the physical parameters of the composite and it is already implemented in commercial FEM software like ABAQUS. But contrary to more advanced criteria, it can't predict different failure modes and the failure predictions are less precise [96, 97].

6 Conclusion

When comparing the fibre volume content of continuous fibre-reinforced thermoplastics discussed in this paper (30–35%) with those of conventional thermosetting composites (60–70%), the limiting factor for the mechanical

Table 5 Overview of element-wise and curve-based designs for the optimisation of fibre-reinforced plastics

Approach	Source
<i>Element-wise designs</i>	
The material orientation of a structure represented by a mesh was optimised to achieve maximum stiffness	Kiyono et al. [84]
The discrete material optimisation (DMO) method, which makes use of a matrix containing a limited pre-defined number of fibre orientations, is extended to take stress and strain-based failure criteria into account	Lund [83]
By limiting the fibre orientations to 0° , $\pm 45^\circ$ and 90° , the shape functions with penalisation (SFP) method, the number of design variables is further reduced	Bruyneel [85]
A bi-value coding parameterisation scheme is used to determine the layer orientation for large-scale design problems	Gao et al. [87]
The modelling of a curvilinear continuous reinforcement for structures with geometric discontinuities, such as holes and notches, is described	Malakhov et al. [88]
To optimise the critical buckling temperature and strain energy the element-wise fibre orientation was parameterised with an angle continuity constraint over the mesh in place	Vijayachandran et al. and Acar et al. [80, 81]
<i>Curve-based designs</i>	
The multi-scale two-level (MS2L9) strategy, which first determines the optimal laminate stiffness properties and then the optimum fibre paths, is used to maximise the first buckling factor of a VAT plate	Montemurro and Catapuno [93]
The fibre paths in a single-ply composite were optimised using streamlines of the perfect flow	Yamanaka et al. [92]
A family of parameterised curves is used to put the fibre paths along the principal stress trajectories. This method was used to optimise a plate with a hole	Zhu et al. [89]
By modelling the laminate as a Mindlin shell and the fibre as path functions, the stiffness was maximised. Manufacturability is considered by examining the curvature and parallelism of fibre paths	Huang et al. [90]
To maximise the stiffness, the fibre paths were optimised using a level-set method	Lemaire et al. [94]
An aeronautical lug which is under tension and compression load is optimised using parameterised cubic spline interpolations representing the fibres. The failure mode was evaluated using Hashin's criteria	Ferreira et al. [91]
The finite element method in combination with Abaqus' integrated Hashin's interlaminar damage initiation theory was used to determine the elastic properties of uni- and biaxial reinforced tokens	Adabi et al. [41]

performance is quickly found. Furthermore, air inclusions as well as the poor adhesion between layers decrease the mechanical performance. This was confirmed by the low interlaminar shear strength which is an indicator for the poor bonding performance between layers.

A summary of the mechanical properties can be found in Table 6. The huge difference between the determined values is caused by the fact that the different authors used test tokens that consisted of reinforced layers mixed with non-reinforced ones (most likely to keep the costs down).

The only author that tested samples with 100% reinforced was Todoroki et al. [51]. They determined a tensile strength of 700 MPa and a Young's modulus of 61 GPa for continuous carbon fibre reinforcement which based on the low fibre content are plausible values. As for the glass fibre-reinforced parts, a UTS of up to 550 MPa and a Young's modulus of 25 GPa can be achieved. All the tested Kevlar samples contained only a few reinforced layers and therefore a very low fibre volume fraction thus no conclusion can be made towards their ultimate mechanical properties. Since

both Dickson et al. and Adabi et al. tested Kevlar and glass fibre samples in an identical setup it can be said that the ultimate tensile strength is very likely the same and the Young's modulus of the Kevlar fibres is 30% higher [40, 41]. This would be in accordance with performance data provided by the manufacturer [98]. Since no glass fibre/Kevlar parts with 100% reinforcement were tested, no definite comparison between them and the continuous carbon fibre reinforcement can be made. But based on the results from the previous research, the carbon fibre filament seems to be 22% stronger and 59% stiffer than the glass fibre filament. The continuous carbon fibre reinforced reinforcement has a flexural strength of 485 MPa which is two and a half times that of the glass fibre reinforcement and more than three times than that of the Kevlar reinforcement. While these conclusions are based on very limited data, it seems like the carbon fibre filament outperforms both the glass fibre and the Kevlar filament regarding the tensile and flexural performance. No comparison can be made regarding the shear strength and strength perpendicular to the fibres (X2/

Table 6 Summary of the mechanical properties of the continuous carbon, glass and Kevlar fibre filament

Carbon fibre			Glass fibre			Kevlar fibre		
UTS (X1) (MPa)	Elastic modulus (MPa)	Source	UTS (X1) (MPa)	Elastic modulus (MPa)	Source	UTS (X1) (MPa)	Elastic modulus (MPa)	Source
216	7730	[40]	444	–	[40]	80	9001	[39]
968	62,500	[47]	450	7200	[44]	164	4370	[40]
304	23,700	[49]	574	25,860	[45]	150	8700	[41]
493	45,200	[50]	140	6400	[41]			
600	13,000	[44]						
701	60,900	[51]						
330	37,000	[41]						
UTS (X2) (MPa)	Elastic modulus (MPa)	Source	UTS (X2) (MPa)	Elastic modulus (MPa)	Source	UTS (X2) (MPa)	Elastic modulus (MPa)	Source
19	3970	[51]	9,84	1130	[45]			
16	3766	[50]						
Compression strength (X1) (MPa)	Compression modulus (MPa)	Source	Compression strength (X1) (MPa)	Compression modulus (MPa)	Source	Compression strength (X1) (MPa)	Compression modulus (MPa)	Source
223	53,000	[45]	82	19,490	[45]			
317	51,198	[50]						
Compression strength (X2) (MPa)	Compression modulus (MPa)	Source	Compression strength (X2) (MPa)	Compression modulus (MPa)	Source	Compression strength (X2) (MPa)	Compression modulus (MPa)	Source
42	–	[45]	12,73	–	[45]			
Flexural strength (MPa)	Flexural modulus (MPa)	Source	Flexural strength (MPa)	Flexural modulus (MPa)	Source	Flexural strength (MPa)	Flexural modulus (MPa)	Source
250	13,020	[40]	196	4210	[40]	125.8	6650	[40]
485	41,600	[47]	149	14,700	[44]			
430	38,100	[44]						
Shear strength (MPa)	Shear modulus (MPa)	Source	Shear strength (MPa)	Shear modulus (MPa)	Source	Shear strength (MPa)	Shear modulus (MPa)	Source
31	2260	[47]	67,77	880	[45]			
35	1803	[50]						
90	2270	[51]						

X3 direction) because there are not enough data available. Due to the inadequate testing standards that led to failure in geometric weak spots as well as the limited data obtained, no conclusion can be made towards the life expectancy under variable loading.

7 Future research needs

For most thin walled parts, the poor adhesion between layers, and therefore, low UTS in layup direction as well as the low Interlaminar shear strength should not be a problem. But for thicker parts, it is relevant, and therefore, should be addressed.

Furthermore, almost no research was done regarding the failure under combined loads. Due to this fact, the materials discussed in this study cannot be used for lightweight applications yet. Since certain damage mechanism may cause premature failure. This risk is usually taken care off by multiplying the actual load with a safety factor and designing the part in a way that it can handle those exaggerated loads. That way the costs of comprehensive testes are avoided but the final product will be heavier. When it comes to ultralightweight design, the goal is to reduce the safety factor to a minimum. To achieve this, the methods and theories used in the design process must be very accurate. Therefore, a very accurate failure theory, that can precisely predict the failure under combined loads, would allow for the more widespread use of this material in lightweight applications.

Funding Open Access funding enabled and organized by Projekt DEAL. This research did not receive any specific grant from funding agencies in the public, commercial, or not-for-profit sectors.

Declarations

Conflict of interest The author declare that they have no conflict of interest.

Open Access This article is licensed under a Creative Commons Attribution 4.0 International License, which permits use, sharing, adaptation, distribution and reproduction in any medium or format, as long as you give appropriate credit to the original author(s) and the source, provide a link to the Creative Commons licence, and indicate if changes were made. The images or other third party material in this article are included in the article's Creative Commons licence, unless indicated otherwise in a credit line to the material. If material is not included in the article's Creative Commons licence and your intended use is not permitted by statutory regulation or exceeds the permitted use, you will need to obtain permission directly from the copyright holder. To view a copy of this licence, visit <http://creativecommons.org/licenses/by/4.0/>.

References

- Zhang X, Chen Y, Hu J (2018) Recent advances in the development of aerospace materials. *Prog Aersp Sci* 97:22–34
- Jin-Woo K, Deon-Gi L (2010) Effect of fiber orientation and fiber contents on the tensile strength in fiber-reinforced composites. *J Nanosci Nanotechnol* 10(5):3650–3653
- Gao W, Zhang Y, Ramanujan D, Ramani K, Chen Y, Williams CB, Wang CC, Shin YC, Zhang S, Zavattieri PD (2015) The status, challenges, and future of additive manufacturing in engineering. *Comput Aided Des* 69:65–89
- Bacciaglia A, Ceruti A, Liverani A (2019) Additive manufacturing challenges and future developments in the next ten years. In: International conference on design, simulation, manufacturing: the innovation Exchange, Modena
- Markforged, “Markforged Mark Two,” Markforged, [Online]. <https://markforged.com/mark-two/>. Accessed 28 May 2020
- Anisoprint, “Anisoprint Composer,” Anisoprint, [Online]. <https://anisoprint.com/product-composer>. Accessed 28 May 2020
- Desktop Metal, “Fibre series,” Desktop Metal, [Online]. <https://www.desktopmetal.com/products/fiber>. Accessed 28 May 2020
- CEAD, “CFAM Prime,” CEAD, [Online]. <https://cead-am.com/wp-content/uploads/2019/09/FOLDER-CFAM.pdf>. Accessed 28 May 2020
- Wicks SS, de Villoria GR, Wardle BL (2010) Interlaminar and intralaminar reinforcement of composite laminates with aligned carbon nanotubes. *Compos Sci Technol* 70(1):20–28
- Czabaj MW, Ratcliffe JG (2013) Comparison of intralaminar and interlaminar mode I fracture toughnesses of a unidirectional IM7/8552 carbon/epoxy composite. *Compos Sci Technol* 89:15–23
- Goel A, Chawla K, Vaidya U, Chawla N, Koopman M (2009) Characterization of fatigue behavior of long fiber reinforced thermoplastic (LFT) composites. *Mater Charact* 60(6):537–544
- Bhuiyan FH, Fertig RS (2017) A physics-based combined creep and fatigue methodology for fiber-reinforced polymer composites. In: 58th AIAA/ASCE/AHS/ASC structures, structural dynamics, and materials conference, Texas
- Eftekhari M, Fatemi A (2017) Variable amplitude fatigue behavior of neat and short glass fiber reinforced thermoplastics. *Int J Fatigue* 98:176–186
- ASTM D3039/D3039M-17 (2017) Standard Test Method for Tensile Properties of Polymer Matrix Composite Materials, ASTM International, West Conshohocken. www.astm.org
- ASTM D6641/D6641M-16e1 (2016) Standard Test Method for Compressive Properties of Polymer Matrix Composite Materials Using a Combined Loading Compression (CLC) Test Fixture, ASTM International, West Conshohocken. www.astm.org
- ASTM D3410/D3410M-16 (2016) Standard Test Method for Compressive Properties of Polymer Matrix Composite Materials with Unsupported Gage Section by Shear Loading, ASTM International, West Conshohocken. www.astm.org
- ASTM D6484/D6484M-14 (2014) Standard Test Method for Open-Hole Compressive Strength of Polymer Matrix Composite Laminates, ASTM International, West Conshohocken. www.astm.org
- ASTM D5766/D5766M-11 (2018) Standard Test Method for Open-Hole Tensile Strength of Polymer Matrix Composite Laminates, ASTM International, West Conshohocken. www.astm.org
- ASTM D6742/D6742M-17 (2017) Standard Practice for Filled-Hole Tension and Compression Testing of Polymer Matrix Composite Laminates, ASTM International, West Conshohocken. www.astm.org
- ASTM D6264/D6264M-17 (2017) Standard Test Method for Measuring the Damage Resistance of a Fiber-Reinforced Polymer-Matrix Composite to a Concentrated Quasi-Static Indentation Force, ASTM International, West Conshohocken. www.astm.org
- ISO 527-4:1997: Plastics—Determination of tensile properties—Part 4: Test conditions for isotropic and orthotropic fibre-reinforced plastic composites, Geneva. www.iso.org
- ISO 12817:2013 Fibre-reinforced plastic composites—Determination of open-hole compression strength, Geneva. www.iso.org
- ISO 14126:1999, Fibre-reinforced plastic composites—Determination of compressive properties in the in-plane direction, Geneva. www.iso.org
- ISO 11566:1996 Carbon fibre—Determination of the tensile properties of single-filament specimens, Geneva. www.iso.org
- ASTM D5379/D5379M-19 (2019) Standard Test Method for Shear Properties of Composite Materials by the V-Notched Beam Method, ASTM International, West Conshohocken. www.astm.org
- ASTM D2344/D2344M-16 (2016) Standard Test Method for Short-Beam Strength of Polymer Matrix Composite Materials and Their Laminates, ASTM International, West Conshohocken. www.astm.org
- ASTM D3518/D3518M-18 (2018) Standard Test Method for In-Plane Shear Response of Polymer Matrix Composite Materials by Tensile Test of a $\pm 45^\circ$ Laminate, ASTM International, West Conshohocken. www.astm.org
- ASTM D5467/D5467M-97 (2017) Standard Test Method for Compressive Properties of Unidirectional Polymer Matrix Composite Materials Using a Sandwich Beam, ASTM International, West Conshohocken. www.astm.org
- ASTM D4255/D4255M-15a (2015) Standard Test Method for In-Plane Shear Properties of Polymer Matrix Composite Materials by the Rail Shear Method, ASTM International, West Conshohocken. www.astm.org
- ASTM D3846-08 (2015) Standard Test Method for In-Plane Shear Strength of Reinforced Plastics, ASTM International, West Conshohocken. www.astm.org

31. ISO 14130:1997 Fibre-reinforced plastic composites—Determination of apparent interlaminar shear strength by short-beam method, Geneva. www.iso.org
32. ISO 14129:1997 Fibre-reinforced plastic composites—Determination of the in-plane shear stress/shear strain response, including the in-plane shear modulus and strength, by the plus or minus 45 degree tension test method, Geneva. www.iso.org
33. ISO 15310:1999 Fibre-reinforced plastic composites—Determination of the in-plane shear modulus by the plate twist method, Geneva. www.iso.org
34. ASTM D7264/D7264M-15 (2015) Standard Test Method for Flexural Properties of Polymer Matrix Composite Materials, ASTM International, West Conshohocken. www.astm.org
35. ASTM D6272-17 (2017) Standard Test Method for Flexural Properties of Unreinforced and Reinforced Plastics and Electrical Insulating Materials by Four-Point Bending, ASTM International, West Conshohocken. www.astm.org
36. ASTM D6415/D6415M-06a (2013) Standard Test Method for Measuring the Curved Beam Strength of a Fiber-Reinforced Polymer-Matrix Composite, ASTM International, West Conshohocken. www.astm.org
37. ISO 14125:1998 Fibre-reinforced plastic composites—Determination of flexural properties, Geneva. www.iso.org
38. ASTM D3479/D3479M-19 (2019) Standard Test Method for Tension-Tension Fatigue of Polymer Matrix Composite Materials, ASTM International, West Conshohocken. www.astm.org
39. Melenka GW, Cheung BK, Schonfield JS, Dawson MR, Carey JP (2016) Evaluation and prediction of the tensile properties of continuous fiber-reinforced 3D printed structures. *Compos Struct* 153:866–875
40. Dickson AN, Barry JN, McDonnell KADDP (2017) Fabrication of continuous carbon, glass and Kevlar fibre reinforced polymer composites using additive manufacturing. *Addit Manuf* 16:146–152
41. Adabi HA, Thai H-T, Paton-Cole V, Patel V (2018) Elastic properties of 3D printed fibre-reinforced structures. *Compos Struct* 193:8–18
42. Scrocco M, Chamberlain T, Chow C, Weinreber L, Ellks E, Halford C, Cortes P, Conner B (2018) Impact testing of 3D printed Kevlar-reinforced onyx material. In: 29th annual international solid freeform fabrication symposium, Austin
43. ASTM E23-18 (2018) Standard Test Methods for Notched Bar Impact Testing of Metallic Materials, ASTM International, West Conshohocken. www.astm.org
44. Goh G, Dikshit V, Nagalingam A, Goh G, Agarwala S, Sing S, Wei J, Yeong W (2018) Characterization of mechanical properties and fracture mode of additively manufactured carbon fiber and glass fiber reinforced thermoplastics. *Mater Des* 137:79–89
45. Justo J, Távara L, García-Guzmán L, París F (2018) Characterization of 3D printed long fibre reinforced composites. *Compos Struct* 185:537–548
46. Dickson AN, Barry JN, McDonnell KA, Dowling DP (2017) Fabrication of continuous carbon, glass and Kevlar fibre reinforced polymer composites using additive manufacturing. *Addit Manuf* 16:146–152
47. Blok L, Longana M, Yu H, Woods BKS (2018) An investigation into 3D printing of fibre reinforced thermoplastic composites. *Addit Manuf* 22:176–186
48. van der Klift F, Koga Y, Todoroki A, Ueda M, Hirano Y, Matsuzaki R (2016) 3D printing of continuous carbon fibre reinforced thermo-plastic (CFRTP) tensile test specimens. *Open J Compos Mater* 6:18–27
49. Lozada JN, Ahuett-Garza H, Orta-Castañón P, Verbeeten WM, Sáiz-González D (2019) Tensile properties and failure behavior of chopped and continuous carbon fiber composites produced by additive manufacturing. *Addit Manuf* 26:227–241
50. Dutra TA, Ferreira RTL, Resende HB, Guimarães A (2019) Mechanical characterization and asymptotic homogenization of 3D-printed continuous carbon fiber-reinforced thermoplastic. *J Braz Soc Mech Sci Eng.* <https://doi.org/10.1007/s40430-019-1630-1>
51. Todoroki A, Oasada T, Mizutani Y, Suzuki Y, Ueda M, Matsuzaki R, Hirano Y (2019) Tensile property evaluations of 3D printed continuous carbon fiber reinforced thermoplastic composites. *Adv Compos Mater* 29(2):147–162
52. Zhang J, Zhou Z, Zhang F, Tan Y, Tu Y, Yang B (2020) Performance of 3D-printed continuous-carbon-fiber-reinforced plastics with pressure. *Materials* 13(2):471
53. Caminero MA, Chacón JM, García-Moreno I, Reverte JM (2018) Interlaminar bonding performance of 3D printed continuous fibre reinforced thermoplastic composites using fused deposition modelling. *Polym Testing* 68:415–423
54. Imeri A, Fidan I, Allen M, Wilson DA, Canfield S (2018) Fatigue analysis of the fiber reinforced additively manufactured objects. *Int J Adv Manuf Technol* 98:2717–2724
55. ASTM D7791-17 (2017) Standard Test Method for Uniaxial Fatigue Properties of Plastics, ASTM International, West Conshohocken. www.astm.org
56. Pertuz AD, Díaz-Cardona S, González-Estrada OA (2020) Static and fatigue behaviour of continuous fibre reinforced thermoplastic composites manufactured by fused deposition modelling technique. *Int J Fatigue* 130:105275
57. Höhne G, Hemminger WF, Flammersheim H-J (2003) Differential scanning calorimetry. Springer-Verlag, Berlin Heidelberg
58. Menard KP (2002) Dynamic mechanical analysis: a practical introduction. CRC Press, Boca Raton
59. Haines PJ (1995) Thermal methods of analysis. Springer, Dordrecht
60. Alemán J, Chadwick A, He J, Hess M, Horie K, Jones R, Kratochvíl P, Meisel I, Mita I, Moad G, Penczek S, Stepto RF (2007) Definitions of terms relating to the structure and processing of sols, gels, networks, and inorganic-organic hybrid materials (IUPAC Recommendations 2007). *Pure Appl Chem* 79(10):1801–1829
61. ASTM D3171-15 (2015) Standard Test Methods for Constituent Content of Composite Materials, ASTM International, West Conshohocken. www.astm.org
62. ASTM D2734-16 (2016) Standard Test Methods for Void Content of Reinforced Plastics, ASTM International, West Conshohocken. www.astm.org
63. Garcea S, Wang Y, Withers P (2018) X-ray computed tomography of polymer composites. *Compos Sci Technol* 156:305–319
64. ASTM D3418-15 (2015) Standard Test Method for Transition Temperatures and Enthalpies of Fusion and Crystallization of Polymers by Differential Scanning Calorimetry, ASTM International, West Conshohocken. www.astm.org
65. ASTM E1356-08 (2014) Standard Test Method for Assignment of the Glass Transition Temperatures by Differential Scanning Calorimetry, ASTM International, West Conshohocken. www.astm.org
66. ISO 11357-1:2016 (2016) Plastics—Differential scanning calorimetry (DSC)—Part 1: General principles, International Organization for Standardization, Geneva. www.iso.org/
67. ISO 11357-2:2020 (2020) Plastics—Differential scanning calorimetry (DSC)—Part 2: Determination of glass transition temperature and step height, Geneva. www.iso.org/
68. ISO 11357-3:2018 (2018) Plastics—Differential scanning calorimetry (DSC)—Part 3: Determination of temperature and enthalpy of melting and crystallization, Geneva. www.iso.org/
69. ISO 11357-4:2014 Plastics—Differential scanning calorimetry (DSC)—Part 4: Determination of specific heat capacity, Geneva. www.iso.org

70. ISO 11357–5:2013 Plastics—Differential scanning calorimetry (DSC)—Part 5: Determination of characteristic reaction-curve temperatures and times, enthalpy of reaction and degree of conversion, Geneva. www.iso.org
71. ASTM D7028–07 (2015) Standard Test Method for Glass Transition Temperature (DMA T_g) of Polymer Matrix Composites by Dynamic Mechanical Analysis (DMA), ASTM International, West Conshohocken. www.astm.org
72. ASTM E1641–18 (2018) Standard Test Method for Decomposition Kinetics by Thermogravimetry Using the Ozawa/Flynn/Wall Method, ASTM International, West Conshohocken. www.astm.org
73. ASTM E1131–20 (2020) Standard Test Method for Compositional Analysis by Thermogravimetry, ASTM International, West Conshohocken. www.astm.org
74. ISO 11358–1:2014 Plastics—Thermogravimetry (TG) of polymers—Part 1: General principles, Geneva. www.iso.org
75. ISO 11667:1997 Fibre-reinforced plastics—Moulding compounds and prepregs—Determination of resin, reinforced-fibre and mineral-filler content—Dissolution methods, International Organization for Standardization, Geneva. www.iso.org
76. ASTM E2533–17e1 (2017) Standard Guide for Nondestructive Testing of Polymer Matrix Composites Used in Aerospace Applications, ASTM International, West Conshohocken. www.astm.org
77. Pascual-González C, Iragi M, Fernández A, Fernández-Blázquez J, Aretxabala L, Lopes C (2020) An approach to analyse the factors behind the micromechanical response of 3D-printed composites. *Compos B Eng* 186:107820
78. Qinghao H, Wang H, Kunkun F, Lin Y (2020) 3D printed continuous CF/PA6 composites: effect of microscopic voids on mechanical performance. *Compos Sci Technol* 191:108077
79. Kawai M, Saito S (2009) Off-axis strength differential effects in unidirectional carbon/epoxy laminates at different strain rates and predictions of associated failure envelopes. *Compos A Appl Sci Manuf* 40(10):1632–1649
80. Vijayachandran A, Acar P, Sundararaghavan V, Waas A (2016) Fiber path optimization of a symmetric laminate with a cutout for thermal buckling, using a novel finite element algorithm. In: *Structures, Structural Dynamics, and Materials Conference*, San Diego
81. Acar P, Vijayachandran A, Sundararaghavan V, Waas A, Rastian M (2016) Optimization of spatially varying fiber paths for a symmetric laminate with a circular cutout under remote uniaxial tension. *SAE Int J Mater Manf* 9(1):75–80
82. Legrand X, Kelly D, Crosky A, Crépin D (2006) Optimisation of fibre steering in composite laminates. *Compos Struct* 75:524–531
83. Lund E (2018) Discrete material and thickness optimization of laminated composite structures including failure criteria. *Struct Multidiscip Optimiz* 57(6):2357–2375
84. Kiyono C, Silva E, Reddy J (2017) A novel fiber optimization method based on normal distribution function with continuously varying fiber path. *Compos Struct* 160:503–515
85. Bruyneel M (2011) SFP—a new parameterization based on shape functions for optimal material selection: application to conventional composite plies. *Struct Multidiscip Optim* 43(1):17–27
86. Bruyneel M, Duysinx P, Fleury C, Gao T (2011) Extensions of the shape functions with penalization parameterization for composite-ply optimization. *AIAA J* 49(10):2325–2329
87. Gao T, Zhang W (2012) A bi-value coding parameterization scheme for the discrete optimal orientation design of the composite laminate. *Numer Methods Eng* 91(1):98–114
88. Malakhov A, Polilov A (2016) Design of composite structures reinforced curvilinear fibres using FEM. *Compos A Appl Sci Manuf* 87:23–28
89. Zhu Y, Liu J, Liu D, Xu H, Yan C, Huang B, Hui D (2017) Fiber path optimization based on a family of curves in composite laminate with a center hole. *Compos B Eng* 111:91–102
90. Huang G, Wang H, Li G (2016) An efficient reanalysis assisted optimization for variable-stiffness composite design by using path functions. *Compos Struct* 153:409–420
91. Ferreira RTL, Ashcroft IA, Li S, Zhuo P (2018) Optimisation of fibre-paths in composites produced by additive manufacturing. In: *6th international conference on engineering optimization*, Lissabon
92. Yamanaka YTAUMHYMR (2016) Fiber line optimization in single ply for 3D printed composites. *Open J Compos Mater* 6:121–131
93. Montemurro M, Catapano A (2017) On the effective integration of manufacturability constraints within the multi-scale methodology for designing variable angle-tow laminates. *Compos Struct* 161:145–159
94. Lemaire E, Zein S, Bruyneel M (2015) Optimization of composite structures with curved fiber trajectories. *Compos Struct* 131:895–904
95. Puck A (1996) *Festigkeitsanalyse von Faser-Matrix-Laminaten*. Carl Hanser Verlag, München Wien
96. Hashin Z (1980) Failure criteria for unidirectional fibre composites. *ASME J Appl Mech* 47(2):329–334
97. Soden P, Hinton M, Kaddour A (1998) A comparison of the predictive capabilities of current failure theories for composite laminates. *Compos Sci Technol* 58:1225–1254
98. Markforged, “Composites Datasheet,” Markforged, 5 10 2019. [Online]. https://static.markforged.com/markforged_composites_datasheet.pdf. Accessed 28 may 2020

Publisher's Note Springer Nature remains neutral with regard to jurisdictional claims in published maps and institutional affiliations.